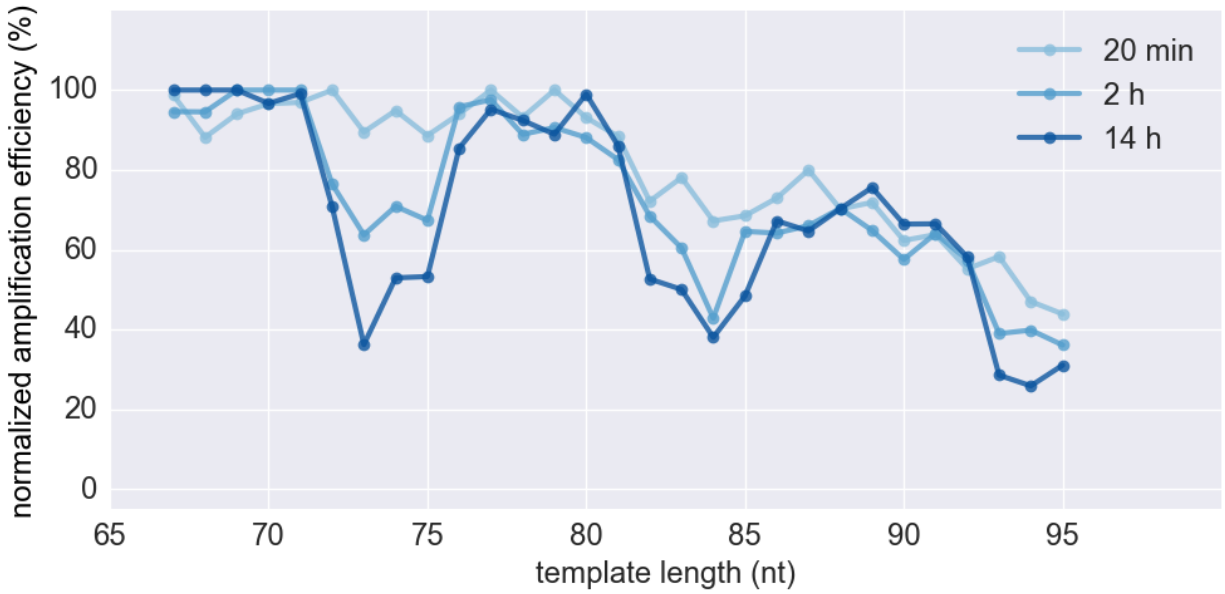

Figure S1. Development of the template length-dependent amplification bias over time. The bias was analyzed for RCA reaction times of 20 min, 2 h and 14 h. After 20 min the minima and maxima are indistinguishable from the statistical noise. Only the overlaid linear decrease towards longer templates can be observed. From two hours onwards the periodic effect becomes more prominent.

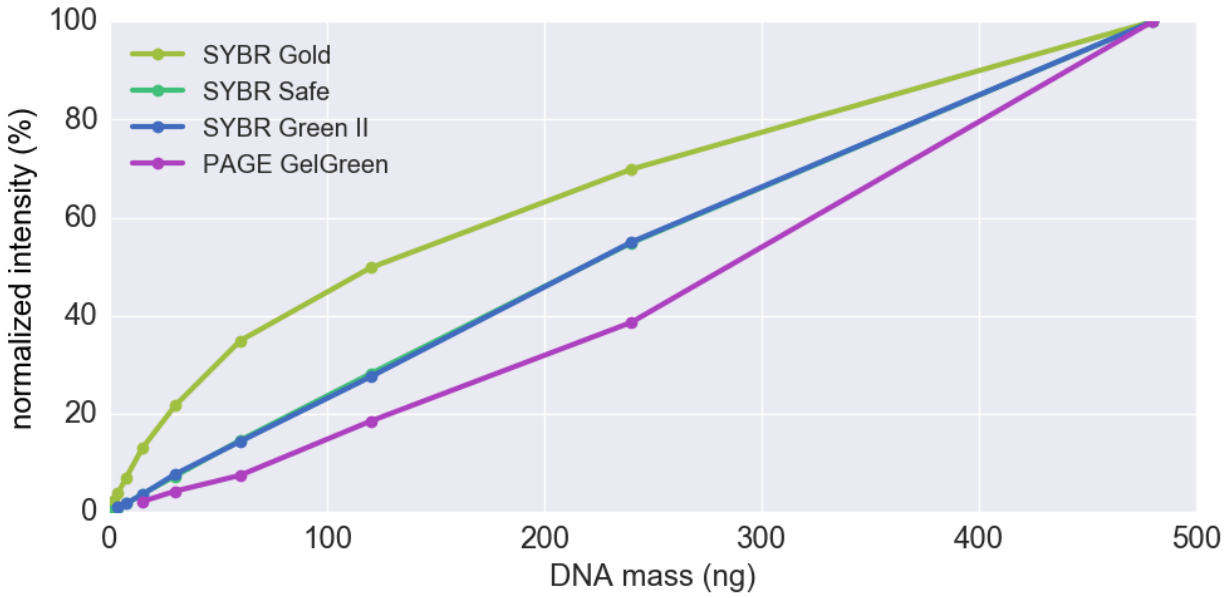

Figure S2. Fluorescence response curves of SYBR Gold, SYBR Safe, SYBR Green II and PAGE GelGreen (Sybr Safe and Sybr Green II are almost identical). The fluorescent intensity after post-staining in response to varying DNA amounts was tested to allow for an exact quantification of gel bands. The investigated oligonucleotide mass range per band was between 0.975 ng and 480 ng. Note that these are normalized intensities; the absolute intensities cannot be directly compared. SYBR Gold was the most sensitive dye at very low amounts, but produced a non-linear response curve. This means that low amounts of DNA appear overrepresented and quantification is problematic. PAGE GelGreen underrepresented low amounts of DNA and the sensitivity was too low below 7.5 ng. Both SYBR Safe and SYBR Green II produced linear response curves. For SYBR Green II, bands could only be quantified from 3.75 ng onwards. SYBR Safe and Sybr Green II had a linear response curve for the entire mass range.

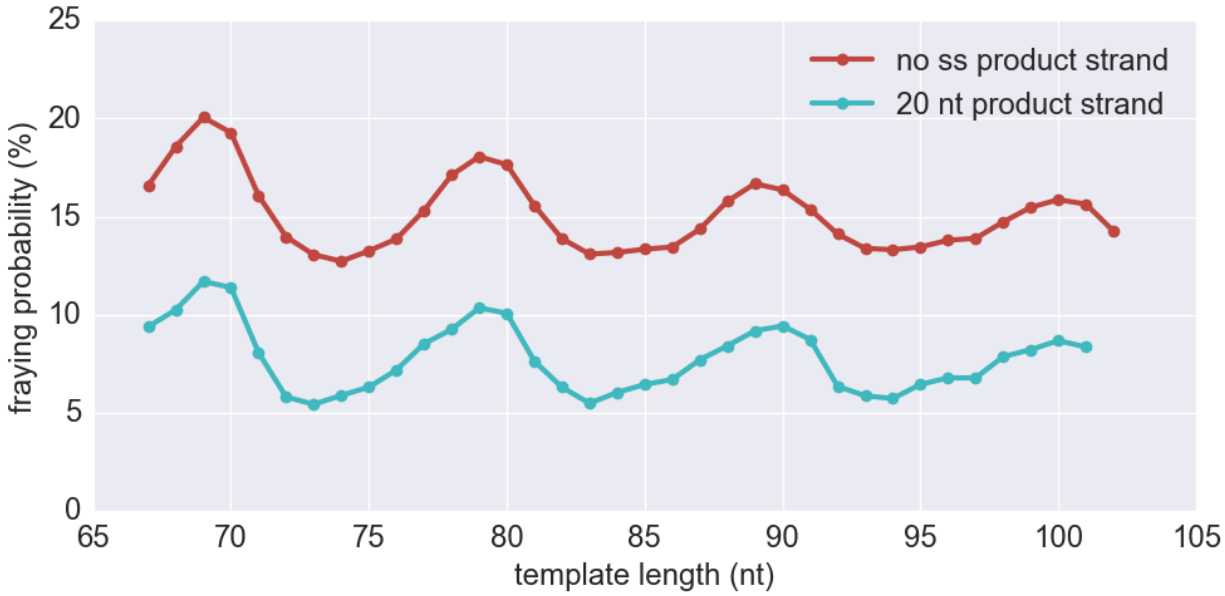

Figure S3. The effect of the product strand on the fraying probability of the first downstream duplex base pair. The product strand stabilizes this base pair (primarily due to the cross-stacking with the first base of the overhang) reducing the baseline propensity to fray. Consequently, the relative difference between maxima and minima increase from a factor of 1.6 to a factor of 2.4 when the product strand is included.

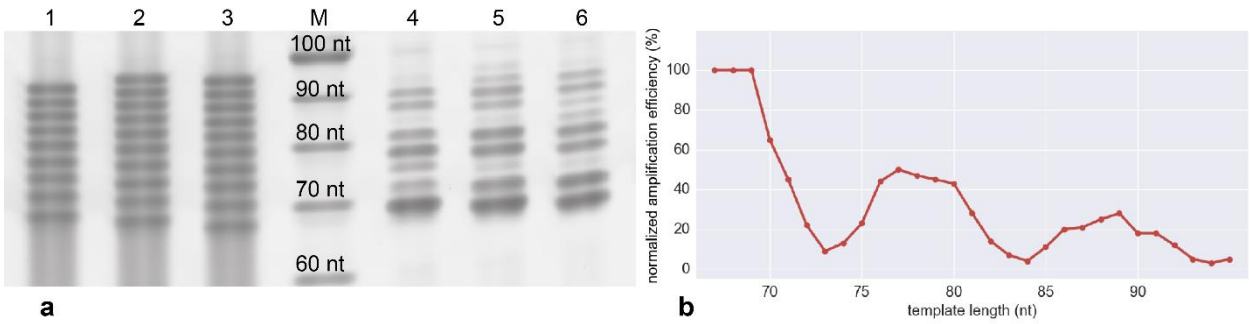

Figure S4. Template length-dependent amplification bias after two rounds of circle to circle amplification. For this, the resulting product of a RCA was cut into monomers, circularized again and another round of RCA was performed as described earlier[1]. (**a**) PAGE scan of the linear pools (lane 1-3) and the amplified oligonucleotides (lanes 4-6). (**b**) Normalized amplification efficiency derived from the gel bands against the template length. This gel was stained with SybrGold, and therefore the amplification differences can be expected to appear even stronger when imaged with SybrSafe (Supplementary Figure 2).

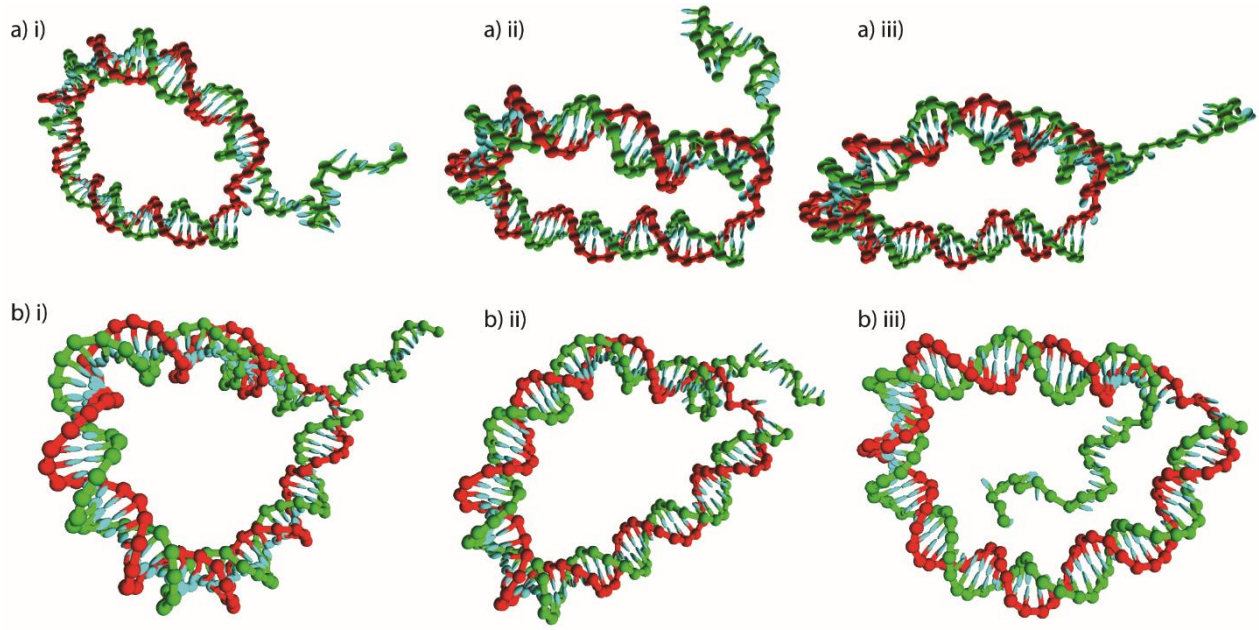

Figure S5. Representative configurations of minicircles obtained from oxDNA molecular dynamics simulations. a) i)-iii) Representative configurations of a 73nt minicircle (amplification and fraying minima). The overhang was never observed to point into the minicircle for minicircle sizes at the minima of amplification bias. b) i)-iii) Representative configurations of an 80nt minicircle (amplification and fraying maxima). The overhang was only rarely observed to point into the minicircle for minicircle sizes at the maxima of the amplification bias. b) iii) An example of a 80nt minicircle configuration where the overhang points into the minicircle.

Note S1. The oxDNA model.

The code is available on sourceforge here: https://sourceforge.net/projects/oxdna/

Parametrised to accurately capture the properties of both dsDNA and ssDNA states, the oxDNA model describes transitions between these states particularly well. For example, the model can very accurately capture the thermodynamics of duplex melting. Furthermore, the model accurately captures the mechanical properties of DNA, the most relevant to the current study being the persistence length and twist modulus of duplex DNA and the relative flexibility of single-stranded DNA[2,3]. Electrostatic interactions are represented by a Debye-Hückel potential, with a variable monovalent salt (NaCl) concentration[3]. Although the model cannot take into account ion-specific effects, at high salt conditions where charges are strongly screened, as is the case experimentally, the behavior only depends weakly on the ionic strength. We choose to use sequence-averaged parameters for the stacking and hydrogen-bonding potentials. This allows us to consider the general effects of minicircle size on fraying, independent of any sequence-specific effects. For example, when examining fraying, a terminal or one-but-terminal GC base-pair would be expected to have a lower fraying propensity than an AT base-pair at the same position. Thus, the use of the sequence-averaged version of oxDNA2 allows minicircles of different sizes to be compared without arbitrarily deciding on the identities of the bases in the region where fraying occurs. Experimentally, this is reflected by the poly-N randomized region of the templates. Furthermore, as the polymerase proceeds around a minicircle it encounters various combinations of base-pairs in the fraying region, and so the experimental amplification rate is expected to be sensitive to the fraying propensity averaged over these sequence environments. The oxDNA2 model allows a "unique topology" to be defined for the base-pairing interactions in a system, i.e. every nucleotide can be specified a single other nucleotide to which it can bind, or be disallowed from binding with any other nucleotides at all. This functionality allows us to avoid transient misbound states, and spend simulation time only sampling states we consider to be relevant for the problem. It also enables us to restrict sections of strands to single-stranded states only, which was used in this study to prevent the overhang from binding at the gap in the minicircle without having to introduce an excluded volume there to represent the polymerase. In the simulations a set of external (to DNA) forces can be applied to nucleotides. In particular, three-dimensional harmonic traps were used in this study to constrain the positions of the centre of mass of some nucleotides, in order to mimic the effect of the bound polymerase on the geometry of the DNA minicircle. Together with the "unique topology" feature, these act as a proxy for the protein, without one explicitly being present in the simulation.

Simulation details. Simulations were performed for nicked minicircles with and without a 20-nucleotide overhang, with the length of the circular strand ranging from 67 to 101 nucleotides. One set of simulations was performed with free minicircles, and another with minicircles where seven of the nucleotides are constrained in three-dimensional harmonic traps to simulate the physical constraints of the polymerase (See Supplementary Figure 5). The relative positions of trapped nucleotides were derived from the X-ray structure of the polymerase with the DNA substrate bound[4]. Hydrogen bond presence/absence between the terminal three base pairs in the direction of the precession of the polymerase is monitored. An established[5] energy criterion of 15% of the maximum hydrogen-bonding energy is used to determine the presence of a base pair (if the hydrogen bonding energy is less than 15% of the maximum hydrogen-bonding energy, the bases are considered unpaired). A criterion twice and half as large was also used, with differences between the three below 0.01% for all systems.

All systems were equilibrated at physiological temperature 310 K and $[Na^+]$ = 0.5 M for 2×10^8 MD steps, with the resulting configuration copied into 16 separate copies that were then decorrelated for 1×10^7 MD steps. Each of the resulting configurations was then used as the starting point for a production run on one CPU core for 120 h or roughly 8×10^8 MD steps each, or roughly 1.3×10^{10} MD steps for each of the 35 systems. The bonding state of the three terminal base pairs on the 5'-end of the non-circular ssDNA strand was recorded every 100 MD steps. The decorrelation time for fraying of the terminal base-pairs is on the order of 10 MD steps in all of the systems.

Supplementary References

1. Schmidt, T. L. *et al.* Scalable amplification of strand subsets from chip-synthesized oligonucleotide libraries. *Nat. Commun.* **6,** 8634 (2015).

2. Ouldridge, T. E., Louis, A. A. & Doye, J. P. K. Structural, mechanical, and thermodynamic properties of a coarse-grained DNA model. *J. Chem. Phys.* **134,** 085101 (2011).

3. Snodin, B. E. K. *et al.* Introducing improved structural properties and salt dependence into a coarse-grained model of DNA. *J. Chem. Phys.* **142,** 234901 (2015).

4. Berman, A. J. *et al.* Structures of phi29 DNA polymerase complexed with substrate: the mechanism of translocation in B-family polymerases. *EMBO J.* **26,** 3494–3505 (2007).

5. Schreck, J. S. *et al.* DNA hairpins destabilize duplexes primarily by promoting melting rather than by inhibiting hybridization. *Nucleic Acids Res.* **43,** 6181–6190 (2015).